31st Annual International Conference of the IEEE EMBS
Minneapolis, Minnesota, USA, September 2-6, 2009

Estimation of Central Aortic Forces in the Ballistocardiogram under Rest and Exercise Conditions

Richard M. Wiard*, *Student Member, IEEE,* Hyun Jin Kim, C. Alberto Figueroa, Gregory T.A. Kovacs, *Fellow, IEEE,* Charles A. Taylor, *Member, IEEE*, and Laurent Giovangrandi, *Member, IEEE*

***Abstract*—The ballistocardiogram (BCG) signal represents the movements of the body in response to cardiac ejection of blood. The BCG signal can change considerably under various physiological states; however, little information exists in literature describing how these forces are generated. A physical analysis is presented using a finite element model of thoracic aortic vasculature to quantify forces generated by the blood flow during the cardiac cycle. The traction at the fluid-solid interface of this deformable wall model generates a Central Aortic Force (CAF) which appears of similar magnitude to recorded BCG forces. The increased pulse pressure in an exercise simulation caused a significant increase in CAF, which is consistent with recent BCG measurements in exercise recovery.**

***Index Terms*—Cardiovascular monitoring, computational modeling, non-invasive diagnostics, hemodynamics**

I. Introduction

BALLISTOCARDIOGRAPHY is a non-invasive method used to assess myocardial strength and estimate changes in cardiac output (CO) [1-3]. The ballistocardiogram (BCG) signal results from the systolic ejection of blood which imparts an upwards force on the vasculature. This BCG force is measured outside the body with systems such as beds [4], chairs [5], and weighing scales [6, 7].

In the literature, there is significant work on the measurement of BCG; however, very little information exists about the genesis of the signal. Noordergraaf explained that the BCG signal results from a change in the center of mass in the body, when blood moves from the ventricles into the greater vessels [8, 9]. The timing of this movement is related to the forces measured. Starr described the BCG as resulting from reactions forces produced when blood circulates in the aortic arch [2, 10]. A change in momentum is produced when blood reverses direction from the ascending to descending segments of the aorta. While these descriptions are helpful for developing intuition, these theories lack a mathematical treatment of how blood flow generates force. We suggest that the origin of the BCG signal is related to fluid-solid interactions in the aorta, and that the primary forces leading to the BCG signal can be mathematically derived by investigating forces at this fluid-solid interface. This work examines the long-held belief of the aorta's role in the BCG signal, using a computational mechanics approach to estimate forces produced during the cardiac cycle.

Manuscript received April 7, 2009.

R.M. Wiard and C.A. Figueroa are with the Bioengineering Department, Stanford University, Stanford, CA 94305 USA (Ph: 650-723-5646; e-mail: rwiard@stanford.edu, cafa@stanford.edu).

H.J. Kim is with the Mechanical Engineering Department, Stanford University, Stanford, CA 94305 USA. (email: kimhj@stanford.edu)

C.A. Taylor is with the Bioengineering Department and Department of Surgery, Stanford University, Stanford, CA 94305 USA.

G.T.A. Kovacs is with the Electrical Engineering Department and Department of Medicine, Stanford University, Stanford, CA 94305 USA.

L. Giovangrandi is with the Electrical Engineering Department, Stanford University, Stanford, CA 94305 USA.

* Denotes corresponding author.

II. Theory

The model presented in this paper considers the aorta as a deformable vessel subject to realistic flow and pressure waves over the cardiac cycle. The reader is directed to [11] for theory of deformable wall mechanics and its realization in Computational Fluid Dynamics (CFD) code. In this paper, we limit the discussion to introducing the concept of *traction* and its proposed relationship to the BCG.

A. Governing Equations

At the fluid-vessel interface, normal forces are acting on the vessel wall. Additionally, a tangential force is present from shear stress caused by viscous flow. The total fluid traction $(\vec{t}^{\,f})$, is the stress vector acting on a surface element of the fluid-vessel wall interface with normal direction $(\vec{n})$ given by:

$$\vec{t}^{\,f} = \vec{t}_{\vec{n}} = \left[-p\underset{\sim}{I} + \underset{\sim}{\tau}\right]\vec{n} \tag{1}$$

where (p) is the scalar pressure quantity, $\underset{\sim}{I}$ is the identity tensor, and the shear tensor $\underset{\sim}{\tau}$ related to the viscosity (μ) and the velocity field $(\vec{v})$ is given by:

$$\underset{\sim}{\tau} = \mu\left(\nabla\vec{v} + (\nabla\vec{v})^T\right) \tag{2}$$

The vessel wall is subjected to an equal and opposite reaction force $\vec{t}^{\,s}$ from the fluid, viz.

$$\vec{t}^{\,f} = -\vec{t}^{\,s} \tag{3}$$

The vessel geometry defines the orientation of the normal vectors. The traction $\vec{t}^{\,f}$ is determined by the governing

equations of motion of the surrounding vessel wall: Young's modulus, wall density, wall thickness, and Poisson's ratio are parameters which describe the response of the vessel.

B. Estimation of the Central Aortic Force

Once a solution for velocity and pressure is obtained from the CFD analysis, fluid-vessel wall traction values are then integrated over the surface area of the aorta. The integral of this traction is defined as the Central Aortic Force (CAF), a vector in three dimensional space. CAF_y is defined as the aortic force projected onto the measurement axis of the BCG. The BCG, as described by Starr, represents the heart-induced body movements along the longitudinal axis (headward-to-footward). The subscript (y) delineates this measurement axis as described in [12].

$$CAF_y \equiv \left[\int_{SA\_aorta} \vec{t}^{\,s} dS \right] \cdot \vec{n}_y \qquad (4)$$

III. Methods

A. Subject-Specific Thoracic Aorta Model

The computer model used in these simulations was constructed from cardiac-gated computer tomography (CT) data of a 36-year-old healthy subject as shown in Fig. 1. The model started from the root of the aorta, ended above the diaphragm, and included major coronary arteries (left anterior descending, left circumflex, and right coronary arteries) and major upper branch vessels (right subclavian, left subclavian, right vertebral, left vertebral, right carotid, and left carotid arteries).

Blood flow was modeled using the incompressible Navier-Stokes equations, and the motion of the vessel wall using the elastodynamics equations [11]. A stabilized finite element method was used to compute pressure and velocity fields in the three-dimensional model of the aorta with coronary arteries and major upper branch vessels. A fixed fluid mesh and small displacements of the vessel wall was assumed [11].

B. Boundary Conditions

Appropriate boundary conditions need to be assigned to compute physiologically realistic velocity and pressure fields in the computational models. A lumped parameter heart model was coupled to the inlet of a three-dimensional thoracic aorta model to compute left ventricular pressure and aortic pressure and flow, by considering the interactions between the heart and arterial system [13]. Left ventricular pressure and volume are related using a time varying elastance function scaled from a normalized elastance function [13]. The coronary outlets are coupled to lumped parameter coronary vascular models whereas the outlets of the upper branch vessels and the descending thoracic aorta are coupled to three-element Windkessel models to represent

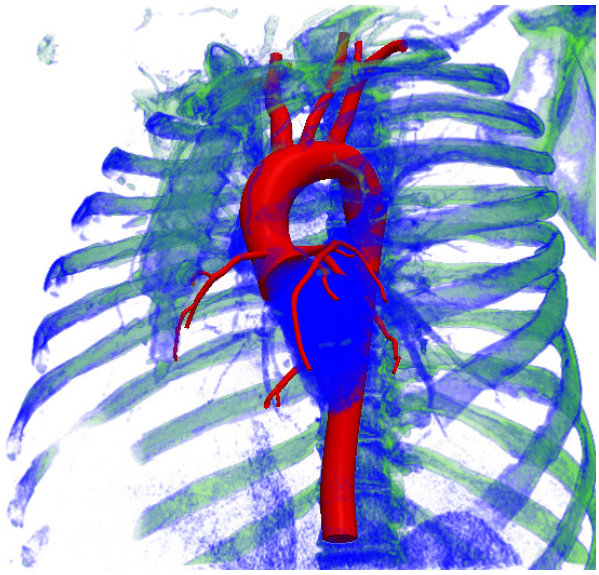

Fig. 1. CT-derived 3D Thoracic Aorta Model (red) of a healthy adult male.

the coronary vascular beds and the upper and lower extremities absent in the computational model, respectively. The parameter values of the heart, coronary, and Windkessel models were set to approximate measured heart rate, CO, and pulse pressure the subject. Finally, an augmented Lagrangian method was used to enforce a shape of the velocity profiles of the inlet and the outlets with retrograde flow [14].

C. Physiological Parameters for Rest and Exercise

The blood vessel walls were modeled with a linear elastic material assumption with Poisson's ratio of 0.5, a wall density of 1.0 g/cm^3, and a uniform wall thickness of 0.1 cm. The Young's modulus of the vessel walls was chosen to be $6.26 \cdot 10^6$ dynes/cm^2 so that the aortic deformations match the measured wall deformations of the CT data. The measured CO of the subject was 5.0 L/min with a heart rate of 60 bpm. To simulate a light exercise condition, the heart rate was doubled to 120 bpm and the downstream resistance of the descending thoracic aorta was reduced to 33% of its resting value, to send more flow to the extremities. This resulted in a CO of 10.3 L/min. The computed brachial pressure of the subject ranged from 78 to 124 mmHg for the resting condition and 78 to 149 mmHg for the exercise condition. The stroke volume increased from 83 cc at rest to 86 cc during exercise. The maximum contractility of the left ventricle maintained the constant value of 2.0 mmHg/cc.

D. Determination of Central Aortic Force

The surface mesh of the model was extracted from the volumetric finite element mesh. Next, the traction values were integrated over the surface area of the aorta to calculate CAF, for each time step. Finally, CAF_y was extracted from

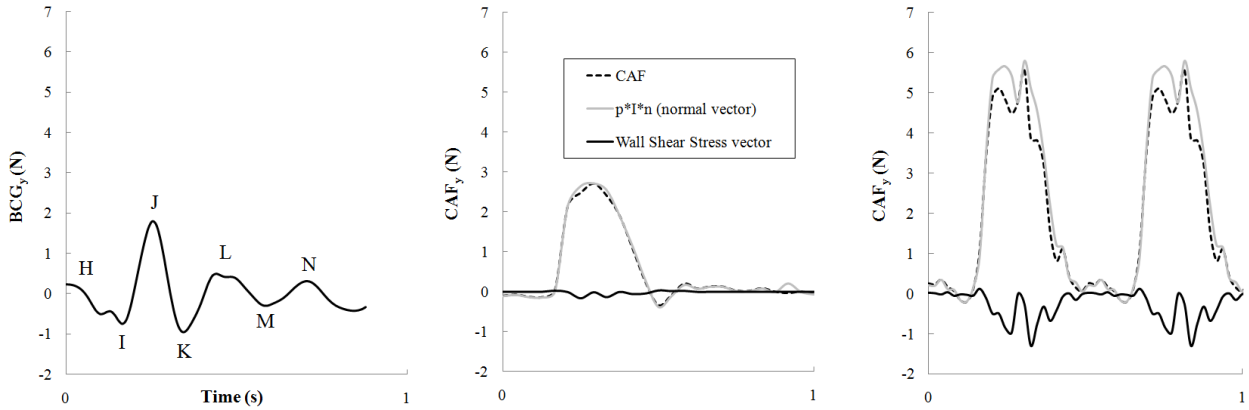

Fig. 2. Typical resting BCG measurement (left). Simulation results of forces produced during rest (center) and exercise (right). Note how the forces generated on the aorta (CAF_y) are similar in magnitude to the BCG measured in [1]. The pulse pressure difference increased the stroke volume from 83 to 86 mL, and doubled CAF peak amplitude.

CAF to estimate the magnitude of the force in the BCG measurement axis. The pressure (normal vector) and wall shear stress terms were derived from CAF_y.

IV. Results and Discussion

A. Central Aortic Forces

Figure 2 shows aortic force time traces for the rest and exercise simulations. The peak-to-peak CAF_y values (dashed traces) for rest and exercise are 3.05 N and 5.77 N, respectively. The $(p\underset{\sim}{I}\cdot\vec{n}_y)$ normal vector is similar to the CAF_y waveform, which suggests that wall shear stress plays a minor role in the overall amplitude for the resting condition. Note that the aortic force plotted is the summation of all the pressure waves of the aorta with time delay due to the deformation of the vessel walls and reflections from the outlets.

B. Comparison to the BCG

The comparison of CAF_y to BCG is limited to data obtained from calibrated BCG recording systems (several works report BCG values with arbitrary units, such as volts or A/D counts). Furthermore, we limit the analysis to BCG measurements in the longitudinal axis, which are often confused with ballistic measurements in the transverse axis (sternal vibrations). The peak force amplitudes of the BCG and CAF_y both occur in early-to-mid systole. The BCG IJ amplitude is the peak amplitude compared to the CAF_y peak amplitudes.

Male subjects in the seminal 20 year study conducted by Starr reported BCG amplitudes of approximately 2.8-4.2 N, recorded on the Starr table-based system [15]. Female BCG amplitudes were approximately 1.4-2.7 N. More recent work on bathroom scale BCG systems by Inan et. al report resting IJ amplitudes of 1.82-2.95 N for males, and 0.83-2.41 N resting values in female subjects [6]. In both studies cited, the recordings were obtained from displacement-based BCG measurement systems and were calibrated in terms of force. BCG amplitudes as high as 8 N were observed after heavy exercise, in exercise recovery studies [1]. In comparison, the estimated CAF_y amplitudes for rest and mild exercise are within ranges previously measured on calibrated BCG recording systems.

The CFD analysis thus predicts force amplitudes that are consistent with BCG amplitudes. Simulation of exercise showed a doubling of the resting CAF_y peak force, also consistent with experimental data. In this case, the increase in pulse pressure accounts for the sharp increase in CAF_y, which relates back to the normal pressure component of traction. CO doubled as well; however, this was mostly due to the doubling of heart rate. While the amplitude of the CAF and BCG forces are similar, which strongly suggests CAF as a major contributor to the BCG signal, it is obvious from Fig. 2 that morphologies are not: the CAF is mostly monophasic, while the BCG is multiphasic. The typical H wave of the BCG was not present in the CAF signal. This wave has been linked to the heart's movement [8], and since our model does not account for that (only the inflow flow profile), it is not expected to appear in these simulations. The BCG K-L-M-N waves are not observed in the CAF traces either. This may be due to geometrical limitations of the model (thoracic aorta only), resonance artifacts from underdamped measurement systems, or more likely due to the propagation of CAF forces through the body [16].

C. Further Observations

The role of the arch was examined by segmenting the thoracic aorta into various pieces and then estimating CAF_y for the individual segments, as shown in Fig 3. Three of the four segments included a portion of the arch, and the fourth segment was just the descending portion after the arch. The semi-circle arch segment lacked the descending aorta, which produced a CAF_y amplitude approximately 110% of the full thoracic model. The quarter-arch segment started at the root of the aorta and ended at the apex. The force was 65% of the full model. The apex-segment, immediately before and after the major upper branch vessels, produced a force 10% of the full model. The descending segment produced a force in the opposite sense of the other segments. We conclude that the

arch is unique to the BCG signal and plays an essential role in the generation of peak forces.

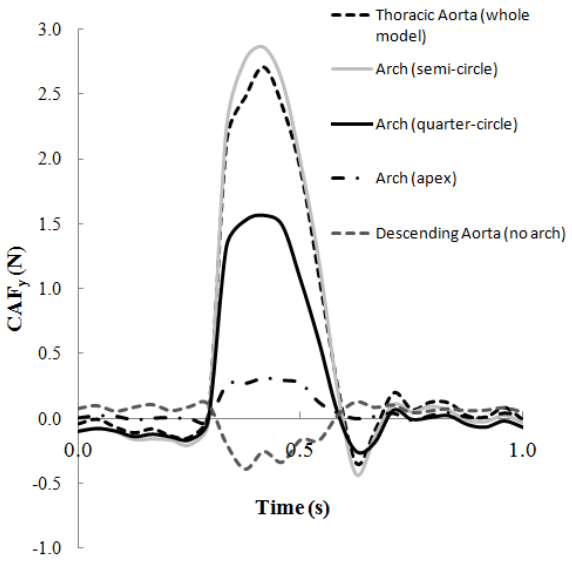

Fig. 3. CAF$_y$ estimates for a sectioned thoracic aorta model. The amplitude quickly died off with segments less than a full arch (quarter, apex, descending).

V. Conclusion

We have demonstrated a mathematical framework to quantify aortic forces with the BCG as an example. Continuum-based approaches give valuable insight into the mechanisms behind the genesis of these cardiovascular forces. This approach creates a flow-to-force transfer function to quantify forces based on vessel geometry and compliance, or by pulse pressure, HR, and downstream impedances. This may help to elucidate what non-invasive BCG signals are capable of measuring related to CO estimation, contractility, and cardiovascular pathology. The aortic arch plays an important role in the development of the peak force, however, this model does not account for all the waves observed in the measured BCG. Pulse wave reflections are present in the systemic arterial tree. These reflections may further contribute to the morphology of the signal. Most importantly, the coupling of the vasculature to the body is not included in this model, and is believed to be a major contributor in the shaping of the BCG signal.

Acknowledgment

The authors thank Omer Inan and Mozziyar Etemadi (Stanford University) for their technical advice and contributions to the project as a whole. The authors gratefully acknowledge the use of the AcuSolve™ linear algebra solver (http://www.acusim.com) and the MeshSim™ automatic mesh generator (http://www.simmetrix.com). This work was supported by the National Institutes of Health (U54 GM072970) and the National Science Foundation (0205741).

References

[1] O. T. Inan, M. Etemadi, A. Paloma, L. Giovangrandi, and G. T. Kovacs, "Non-Invasive Cardiac Output Trending During Exercise Recovery on a Bathroom-Scale-Based Ballistocardiograph," *Physiological Measurement,* vol. 30, pp. 261-274, 2009.

[2] I. Starr, A. J. Rawson, H. A. Schroeder, and N. R. Joseph, "Studies on The Estimation of Cardiac Output in Man, and of Abnormalities in Cardiac Function, From The Heart's Recoil and The Blood's Impacts; The Ballistocardiogram," *The American Journal of Physiology,* vol. 127, pp. 1-28, August 1 1939.

[3] O. T. Inan, M. Etemadi, R. M. Wiard, G. T. A. Kovacs, and L. Giovangrandi, "Non-Invasive Measurement of Valsalva-Induced Hemodynamic Changes on a Bathroom Scale Ballistocardiograph," in *Engineering in Medicine and Biology Society, 2008. EMBS 2008. 30th Annual International Conference of the IEEE*, 2008, pp. 674-677.

[4] H. B. S. a. W. B. T. Maurice B. Rappaport, "Ballistocardiography: I. Physical Considerations," *Circulation,* vol. 7, pp. 229-246, 1953.

[5] A. Akhbardeh, S. Junnila, M. Koivuluoma, T. K. Koivistoinen, and A. Varri, "Evaluation of heart condition based on ballistocardiogram classification using compactly supported wavelet transforms and neural networks," in *IEEE Conference on Controls Applications*, 2005, pp. 843-848.

[6] O. T. Inan, M. Etemadi, R. M. Wiard, L. Giovangrandi, and G. T. Kovacs, "Robust Ballistocardiogram Acquisition for Home Monitoring," *IOP Journal of Physiological Measurement,* vol. 30, pp. 169-185, Jan 16 2009.

[7] J. Williams, "Bridge Circuits - Marrying Gain and Balance," *Linear Technology Application Note,* vol. AN43, pp. 1-46, 1990.

[8] A. Noordergraaf, "Genesis of Displacement of the Human Longitudinal Ballistocardiogram from the Changing Blood Distribution," *American Journal of Cardiology,* pp. 748-756, December 1958.

[9] A. Noordergraff, "Further Studies on a Theory of the Ballistocardiogram," *Circulation,* vol. 23, pp. 413-425, March 1 1961.

[10] I. Starr and H. A. Schroeder, "Ballistocardiogram. II. Normal Standards, Abnormalities Commonly Found in Diseases of the Heart and Circulation, and Their Significance," *Journal of Clinical Investigation,* vol. 19(3), pp. 437–450, May 1940.

[11] C. A. Figueroa, I. E. Vignon-Clementel, K. E. Jansen, T. J. R. Hughes, and C. A. Taylor, "A Coupled Momentum Method for Modeling Blood Flow in Three-Dimensional Deformable Arteries," *Computer Methods in Applied Mechanics and Engineering,* vol. 195, pp. 5685-5706, 2006.

[12] W. R. Scarborough, S. A. Talbot, J. R. Braunstein, M. B. Rappaport, W. Dock, W. F. Hamilton, J. E. Smith, J. L. Nickerson, and I. Starr, "Proposals for Ballistocardiographic Nomenclature and Conventions: Revised and Extended: Report of Committee on Ballistocardiographic Terminology," *Circulation,* vol. 14, pp. 435-450, 1956.

[13] H. J. Kim, I. E. Vignon-Clementel, C. A. Figueroa, J. F. LaDisa, K. E. Jansen, J. A. Feinstein, and C. A. Taylor, "On Coupling a Lumped Parameter Heart Model and a Three-Dimensional Finite Element Aorta Model," *Submitted to the Ann. Biomed. Eng.,* 2008.

[14] H. Kim, C. Figueroa, T. Hughes, K. Jansen, and C. Taylor, "Augmented Lagrangian Method for Constraining the Shape of Velocity Profiles at Outlet Boundaries for Three-dimensional Finite Element Simulations of Blood Flow," *Comp. Methods Appl. Mech. Engng.,* 2009.

[15] I. Starr and F. C. Wood, "Twenty-Year Studies with the Ballistocardiograph: The Relation between the Amplitude of the First Record of "Healthy" Adults and Eventual Mortality and Morbidity from Heart Disease," *Circulation,* vol. 23, pp. 714-732, May 1 1961.

[16] G. Elzinga, N. Westerhof, G. van den Bos, and P. Verdouw, "Transfer of Cardiovascular Forces Through the Body," *Medical and Biological Engineering and Computing,* vol. 12, pp. 322-327, 1974.